T55A-0046

The Mantle Seismic Structure below Canada and Alaska Constrained by a New Absolute P-wavespeed Tomographic Model

[1]M. Liddell, [2*]A. Boyce, [2]S. Pugh, [2]J. Brown, [2]E. McMurchie, [2]A. Parsons, [3]C. Estève, [4]S. Burdick,
[1]F. Darbyshire, [2]S. Cottaar, [5]I. Bastow, [6]A. Schaeffer, [7]P. Audet, [8]D. Schutt and [8]R. Aster

1 Overview

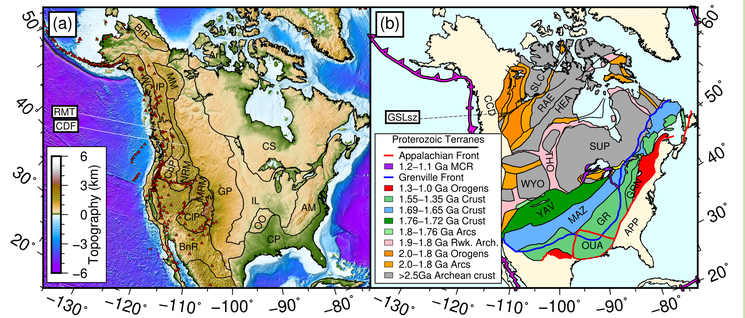

FIGURE 1: (a) North American topography and physiographic provinces. Quaternary volcanism: red triangles. ArP: Arctic Plains, BnR: Basin and Range, BrR: Brooks Range, CbP: Columbia Plateau, CDF: Cordilleran Deformation Front, CIP: Colorado Plateau, CP: Coastal Plain, CS: Canadian Shield, GP: Great Plains, IL: Central Interior Lowlands, IP: Canadian Interior Plateaus, MM: Mackenzie Mountains, MRM: Middle Rocky Mountains, NRM: Northern Rocky Mountains, OO: Ozark-Quachita Highlands, RMT: Rocky Mountian Trench, WC: Western Coastal Pacific Ranges. **(b)** Simplified Proterozoic geology (adapted after Whitmeyer and Karlstrom, 2007). APP: Appalachian terranes, CCD: Canadian Cordillera, GR: Granite-Rhyolite, GRN: Grenville Province, GSLsz: Great Slave Lake Shear Zone, HEA: Hearne Craton, MAZ: Mazatzal, MCR: Mid-Continent Rift, RAE: Rae Craton, Rwk. Arch.: Reworked Archean crust, SLC: Slave Craton, SUP: Superior Caton, THO: Trans-Hudson Orogen, WYO: Wyoming Craton, YAV: Yavapai. Plate boundaries: magenta lines.

- **Mapping P-wavespeeds (V_p) in the Canadian & Alaskan mantle will further our understanding of its formation and evolution.**
- **S-wavespeeds (V_s) are primarily sensitive to temperature while complimentary V_p constraints help reveal compositional variations.**
- **CHALLENGE: How to extract absolute arrival-time measurements from often-noisy data recorded by temporary seismograph networks to ensure that regional Canadian & Alaskan datasets are compatible with complementary continental and global datasets provided by global pick databases.**
- **SOLUTION: Utilize the Absolute Arrival-time Recovery Method (Boyce et al., 2017) to extract >180,000 new absolute arrival-times from land and sea-based seismograph stations across Canada & Alaska.**
- **We combine new data with the latest USArray P-wave arrival-time data from the contiguous US & Alaska. Using an adaptively parameterized least-squares tomographic inversion, we develop an absolute V_p model, focused on Canada & Alaska: CAP21.**

2 Absolute-Arrival Time Data

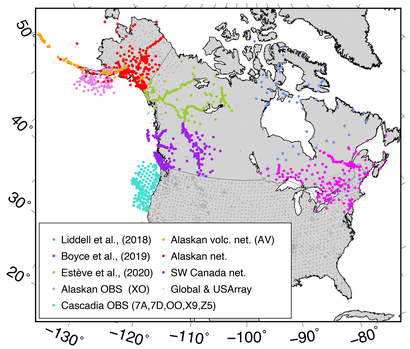

FIGURE 2 (Above): Global, continental and regional seismograph network data sets. Eight regional seismic networks are processed separately and include both land and ocean-bottom seismometers (OBS). Global and USArray network stations: small grey circles.

- Seismograph stations across Canada & Alaska are split into 8 sub-regions to derive P-wave relative arrival-time picks via waveform cross-correlation (Fig. 2). We use existing waveform databases where available e.g., Liddell et al., (2018) & Estève et al., (2020).
- Absolute arrival-times are required to image continental scales (Fig. 3).
- The Absolute Arrival-time Recovery Method (Boyce et al., 2017) is applied to each data set. Building on Boyce et al., (2019), our total data set comprises 202,719 P-wave absolute arrival-times from temporary seismograph stations (2002-2020).
- New data supplemented with global data (Li et al., 2008) and the latest USArray travel time picks (Fig. 4). Global and USArray data include other seismic phases e.g., Pn, Pg, pP, PKP and PKIKP.
- SW Canada; residuals delayed below the Cordillera, but generally early east of the CDF.
- NW Canada; residuals delayed below the Cordillera, but north of the Great Slave Lake shear zone (GSLsz), slow residuals extend eastwards towards the Slave Craton beyond the CDF.
- E Canada; residuals early almost ubiquitously below the Superior craton and N Hudson Bay.

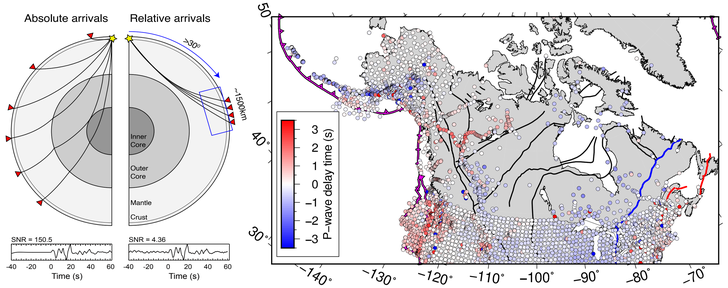

FIGURE 3 (Above left): Schematic of differences between relative and absolute arrival-times, which facilitate comparison with the global mean and whole-mantle imaging.
FIGURE 4 (Above right): Mean P-wave absolute arrival-time residuals. Residuals are derived from the following databases: Global (Li et al., 2008); USArray, BBNAP19 (Boyce et al., 2019); new CAP21 data set added here. Residuals are corrected for Earth's ellipticity and station elevation. Structural boundaries as in Fig. 1.

CAP21 TAKE-HOME MESSAGES

1) **Temporary seismograph networks** greatly **improve resolving power** of absolute **P-wave tomography in Canada & Alaska**.
2) **Fast wavespeeds** characterize **upper mantle** beneath **eastern & northern Canadian cratons**.
3) **SW Canada:** Sharp **wavespeed transition** follows RMT. **NW: Slow wavespeeds** extend eastward of CDF to the **Slave craton**.
4) Slow wavespeeds underlying **kimberlite-rich Slave craton** may reflect **metasomatic modification** caused by ancient subduction.

3 Tomographic Method and Resolution

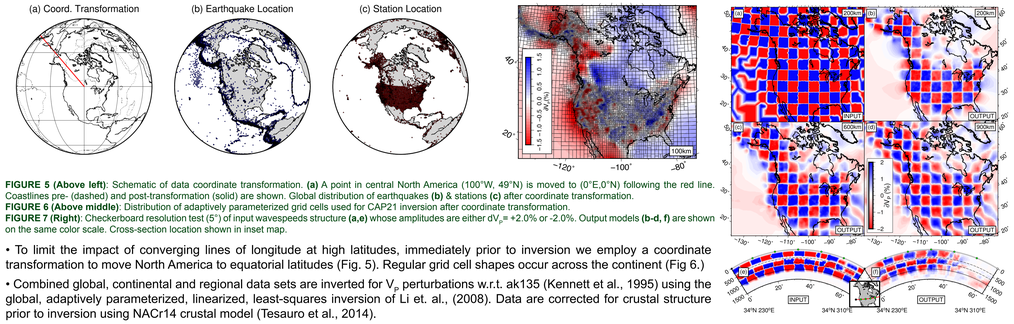

FIGURE 5 (Above left): Schematic of data coordinate transformation. **(a)** A point in central North America (100°W, 49°N) is moved to (0°E,0°N) following the red line. Coastlines pre- (dashed) and post-transformation (solid) are shown. Global distribution of earthquakes **(b)** & stations **(c)** after coordinate transformation.
FIGURE 6 (Above middle): Distribution of adaptively parameterized grid cells used for CAP21 inversion after coordinate transformation.
FIGURE 7 (Right): Checkerboard resolution test (5°) of input wavespeeds structure **(a,e)** whose amplitudes are either dV_p= +2.0% or -2.0%. Output models **(b-d, f)** are shown on the same color scale. Cross-section location shown in inset map.

- To limit the impact of converging lines of longitude at high latitudes, immediately prior to inversion we employ a coordinate transformation to move North America to equatorial latitudes (Fig. 5). Regular grid cell shapes occur across the continent (Fig 6.)
- Combined global, continental and regional data sets are inverted for V_p perturbations w.r.t. ak135 (Kennett et al., 1995) using the global, adaptively parameterized, linearized, least-squares inversion of Li et. al., (2008). Data are corrected for crustal structure prior to inversion using NACr14 crustal model (Tesauro et al., 2014).
- Recovery of 5° checkerboard anomalies below W & SE Canada significantly improved using temporary network data sets. Anomalies of 2° are resolved in the Alaskan upper mantle. Upper mantle resolution below NE Canada improves for features at 7.5°-10° length scales.

4 CAP21 Tomographic Model

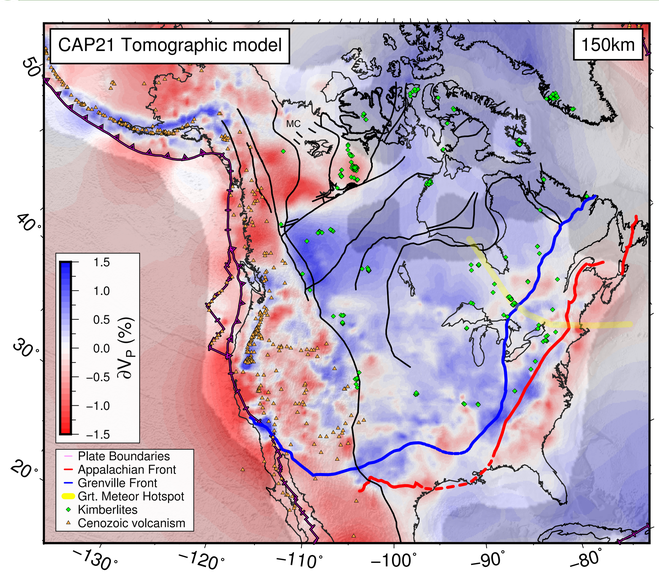

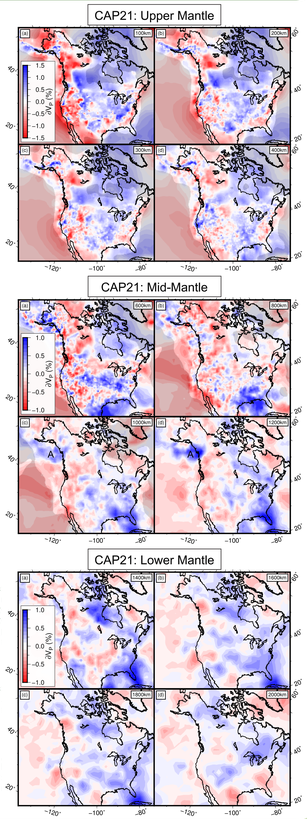

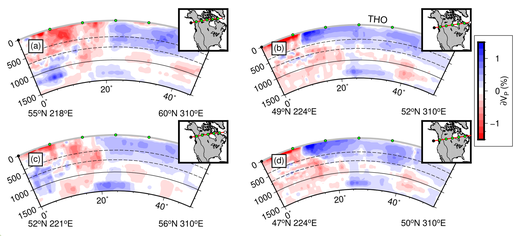

FIGURE 8 (Above): CAP21 tomographic model at 150km depth, plotted as deviation from ak135 over topographic shading. Grey areas are unresolved according to recovery of 5° checkerboard anomalies (following Burdick et al., 2014). Structural boundaries as in Fig. 1. MC: Mackenzie Craton.

FIGURE 9 (Left): CAP21 tomographic model cross sections through Canada. North-to-south (a,c,b,d). Inset maps: cross section locations (red). CDF: black line.

FIGURE 10, 11, 12 (Right Top, Middle, Bottom): CAP21 tomographic model plotted at several upper, mid and lower mantle depths. Grey regions are unresolved as in Fig. 8. Wavespeed scales are variant.

5 Alaskan Upper Mantle Wavespeed Structure

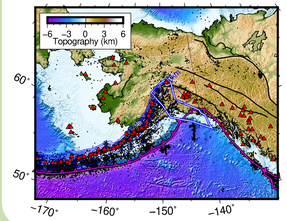

FIGURE 13 (Left): Alaskan tectonics. Plate boundaries: magenta lines, Slab2.0 contours: blue lines (Hayes et al., 2018), $m_b \geq 4.0$ earthquakes 1971-2021: black dots, Quaternary volcanism: red triangles. Subducted Yakutat terrane: blue outline (after Eberhart-Phillips et al., 2006).

FIGURE 14 (Right): CAP21 tomographic model plotted at several depths and cross sections for Alaska. Grey regions are unresolved as in Fig. 8. Yakutat terrane: green outline. Quaternary volcanoes: green triangles.

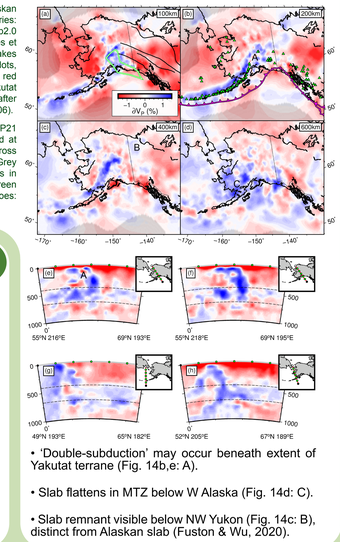

6 CAP21 Model Observations

- Upper mantle wavespeeds in W Canada mirror distribution of absolute arrival-time residuals (Fig. 4). Wavespeed pattern independent of crustal model used, only amplitudes vary.
- Slow upper mantle wavespeeds underlie CCD and MM.
- Fast upper mantle wavespeeds underly all kimberlite localites except in NW Canada.
- Slow wavespeeds beneath SLC support metasomatic modification (e.g., Aulbach et al., 2013; Eeken et al., 2018), perhaps above ancient subduction zones.
- Westward dipping fast wavespeed boundary in SW Canada (Fig. 9b,d) below RMT supports collisional origin of Cordillera (Chen et al., 2019).
- Inconclusive evidence for unexposed Mackenzie craton (Fig. 8) due to lack of overlying stations.
- Kula slab remnant (e.g., Clennett et al., 2020) imaged at ~1000-1200km depth offshore S Alaska and Yukon (Fig. 11c,d: A).
- 'Double-subduction' may occur beneath extent of Yakutat terrane (Fig. 14b,e: A).
- Slab flattens in MTZ below W Alaska (Fig. 14d: C).
- Slab remnant visible below NW Yukon (Fig. 14c: B), distinct from Alaskan slab (Fuston & Wu, 2020).

7 Model Comparisons

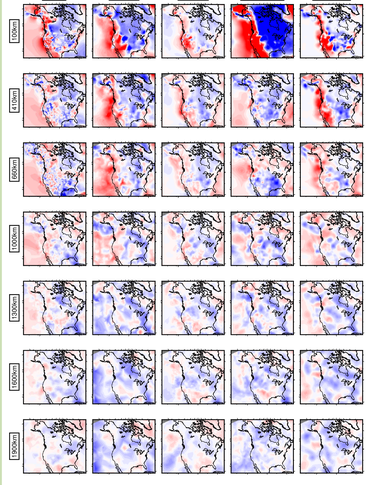

- Global & USArray data insufficient to resolve W & N Canada upper mantle, CAP21 data is crucial here.
- Relationship of wavespeeds to CDF is revealed by CAP21 data.
- Alaskan slab structural complexities revealed by USArray data.
- CAP21 data illuminates long wavelength subduction relics in the mid-mantle below N America.

FIGURE 15 (Below): Influence of different data sets in CAP21 inversion. **Left:** Inversion using only global and USArray Transportable Array (TA) data, **Middle:** Inversion using only new data processed here (CAP21-Only). **Right:** Inversion using all data as in previous figures. **Top:** Recovery of 5° degree checkerboard resolution test (Fig. 7) at 200km depth. **Middle/Bottom:** Output of data inversion from 200-1200km depth. Note variable velocity scale. CDF: black line.

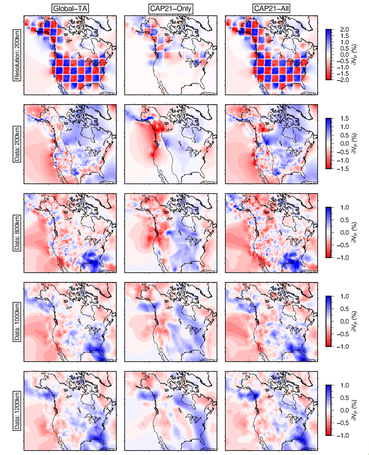

FIGURE 14 (Above): CAP21 tomographic model compared to 4 other global scale P-wave tomographic models PRI-P05 (Montelli et al., 2006), MIT-P08 (Li et al., 2008), LLNL-G3Dv3 (Simmons et al., 2012), DETOX-P2 (Hosseini et al., 2019).

- Pattern of wavespeeds in US upper mantle is broadly similar, amplitudes differ. Differences exist in Canada.
- Previous models do not show slow P-wavespeeds east of the CDF and beneath the SLC due to limited station coverage.
- Models show similarity at ≥1000km depth.

Affiliations:
*[1]Centre de recherche Geotop, Université du Québec à Montréal, QC, Canada. *Present Address: Laboratoire de Géologie de Lyon : Terre, Planète, Environnement, Université Claude Bernard, Lyon1, Bâtiment Géode, 2, rue Raphaël Dubois, 69622 Villeurbanne Cedex, France. [2]Department of Earth Sciences, University of Cambridge, UK. [3]McGill University, Montreal, Canada. [4]Wayne State University, Geology Department, Detroit, MI, USA. [5]Department of Earth Science & Engineering, Imperial College London, UK. [6]Geological Survey of Canada Pacific Division, Sidney, BC, Canada. [7]University of Ottawa, Department of Earth and Environmental Sciences, Ottawa, ON, Canada. [8]Colorado State University, Geosciences Department, Fort Collins, CO, USA.*

Funding statement:
This work was supported by the **Natural Environment Research Council** [NERC grant reference number NE/R010862/1] and the **European Research Council** (ERC) under the European Union's Horizon 2020 research and innovation programme (grant agreement No. 804071 -ZoomDeep). Further support provided by **Centre National de la Recherche Scientifique** at unit UMR5276 (LGL-TPE) and the **Geological Survey of Canada**'s GEM GeoNorth program.

References:
Aulbach S. et al., **(2013)** Nature and timing of metasomatism in the stratified mantle lithosphere beneath the central Slave craton (Canada). Chem Geol 352, 153–169. *Boyce, A. et al., (2017)*, From relative to absolute teleseismic travel-times: the Absolute Arrival-time Recovery Method (AARM), BSSA, 107(5), pp. 2511-2520. Boyce A. et al., **(2019)**, Variable modification of continental lithosphere during the Proterozoic Grenville orogeny: Evidence from teleseismic P-wave tomography, EPSL 525, 115763. Chen, Y. et al., **(2019)** Seismic evidence for a mantle suture and implications for the origin of the Canadian Cordillera. Nature Comms 10, 2249. Clennett, E. et al., **(2020)** A Quantitative Tomotectonic Plate Reconstruction of Western North America and the Eastern Pacific Basin. Gcubed 21. Eberhart-Phillips, D. et al., **(2006)**, Imaging the transition from Aleutian subduction to Yakutat collision in central Alaska, with local earthquakes and active source data. JGR, 111, B11303. Eeken, T. et al., **(2018)** Seismic evidence for depth-dependent metasomatism in cratons. EPSL 491, 148–159. Estève, C. et al., **(2020)** The Upper Mantle Structure of Northwestern Canada From Teleseismic Body-Wave Tomography. JGR 125. Fuston, S. & Wu, J., **(2020)** Raising the Resurrection plate from an unfolded-slab plate tectonic reconstruction of northwestern North America since early Cenozoic time. Gsa Bulletin 133, 1128–1140. Hayes, G. et al., **(2018)**, Slab2, a comprehensive subduction zone geometry model. Science 362, 58–61. Hosseini, K. et al., **(2019)**, Global mantle structure from multifrequency tomography using P, PP and P-diffracted waves. GJI 220, 96–141. Kennett, B. et al., **(1995)**, Constraints on seismic velocities in the earth from traveltimes. GJI. 122, pp. 108-124. Li, C. et al., **(2008)**, A new global model for P wave speed variations in Earth's mantle. Gcubed, 9, Q05018. Liddell M. et al., **(2018)**, Precambrian Plate Tectonics in Northern Hudson Bay: Evidence From P and S Wave Seismic Tomography and Analysis of Source Side Effects in Relative Arrival-Time Data Sets. JGR 123, 5690–5709. Montelli, R. et al., **(2006)**, A catalogue of deep mantle plumes: New results from finite-frequency tomography. Gcubed 7. Simmons, N., et al., **(2012)**, LLNL-G3Dv3: Global P wave tomography model for improved regional and teleseismic travel time prediction. JGR. 117. Tesauro, M. et al., **(2014)**, NACr14: A 3D model for the crustal structure of the North American Continent. Tectonophysics 631, 65–86. Veenstra, E. et al., **(2019)**, The Role of Variable Slab Dip in Driving Mantle Flow at the Eastern Edge of the Alaskan Subduction Margin: Insights From Shear-Wave Splitting. Gcubed. 20, 2433–2448.

alistair.boyce@univ-lyon1.fr / @alistair_boyce